



# Low Temperature Plasma Technology Laboratory

---

## **Time-varying impedance of the sheath on a probe in an RF plasma**

Francis F. Chen

LTP-509

September, 2005



Electrical Engineering Department  
Los Angeles, California 90095-1594

# **Time-varying Impedance of the Sheath on a Probe in an RF Plasma**

Francis F. Chen

*Electrical Engineering Department, University of California, Los Angeles, 90095-1594*

## **ABSTRACT**

Langmuir probes used in radiofrequency (rf) discharges usually include compensation elements that minimize the effect of high frequency oscillations in plasma potential. The design of these elements requires knowledge of the capacitance of the sheath on the probe tip, a quantity which varies nonlinearly during the rf cycle. Sheath capacitance has been studied previously for capacitively coupled discharges, where the rf is applied to the electrodes. Here the problem is treated from the standpoint of a small probe in a fluctuating discharge. This work differs from existing literature in that a) no step model is used, and the Debye sheath is treated exactly; b) the treatment is simple and analytic; c) the time-variation of the capacitance is explicitly shown; d) the results are applied to probe design; and e) cylindrical geometry is considered. The rf frequency is assumed low enough that electron transit times can be ignored. We find that when the rf excursions bring the sheath from the Child-Langmuir region into the Debye sheath or electron saturation region, its capacitance has a strongly nonlinear behavior.

## A. Introduction

In the design of rf-compensated Langmuir probes for measurements in rf plasmas, it is necessary to know the capacitive coupling through the sheath of rf fluctuations in plasma potential. The simple approach normally used is to consider the sheath to be a vacuum capacitor whose thickness is roughly estimated. In plane geometry this thickness is not well defined, even if a sheath edge is well defined, because the thickness depends on the slope of the potential at the edge, and this depends on the transition to the presheath. It is impractical to solve for the presheath, since the solution depends on collisions and ionization and is specific to each discharge. More accurate treatments of rf sheaths can be found in the literature but are not always suitable for the present task.

Lieberman<sup>1,2</sup> has given analytic solutions for the sheath on a driven electrode in a capacitively coupled plasma (CCP). However, he used a model in which the electron density was approximated by a single step. Godyak and Sternberg<sup>3</sup> pointed out that high- and low-frequency approximations can be made depending on whether the rf frequency  $\omega$  is larger or smaller than the ion plasma frequency  $\Omega_p$ , and they solved<sup>4</sup> the high-frequency case for a CCP driven symmetrically relative to ground. How the shape of the sheath changes during the rf cycle was computed numerically by Zhang et al.<sup>5</sup>, with the result that large changes occur in the low-frequency case, the one treated in this paper. However, they did not give the sheath capacitance explicitly.

Godyak<sup>3</sup> showed that the sheath capacitance  $C_{sh}$  depends only on the surface charge on the probe and can be calculated without solving for the sheath thickness numerically. Sudit and Chen<sup>6</sup> used this shortcut to calculate  $C_{sh}$ . In that work, however, they neglected the Debye sheath, treating only the Child-Langmuir (C-L) sheath, adding, rather inconsistently, the Bohm velocity at the sheath edge. Here we solve the plane sheath problem consistently, showing exactly what approximations were previously made, and also obtaining formulas from which the sheath capacitance can be calculated even when the probe is not biased far from the space potential. To establish notation, we start with a brief review of plane sheath theory before applying it to the calculation of sheath capacitance as a function of time. Cylindrical sheaths and the resistive part of the sheath impedance will be treated at the end.

## B. Plane sheaths in a nutshell

### 1. Basic equations

We start by defining a sheath edge  $s$  (Fig. 1) with  $V_s$ ,  $n_s$ , and  $v_s$  denoting respectively the potential, density, and ion velocity there. Following traditional practice, we set  $V_s = 0$  in the absence of rf, and assume quasineutrality up to  $s$  so that  $n_i(s) = n_e(s) \equiv n_s$ . The ions enter the sheath with a unidirectional, monoenergetic velocity  $v_s$ , whose Bohm value will be recovered in due course. There is no artificial separation between the Debye sheath (where  $n_e \neq 0$ ) and the Child-Langmuir sheath (where  $n_e = 0$ ). Defining

$$V = \tilde{V} - V_s, \quad (1)$$

where  $\tilde{V}$  is the actual potential as  $V_s$  varies, we write Poisson's equation as

$$\epsilon_0 \frac{d^2 V}{dx^2} = e(n_e - n_i). \quad (2)$$

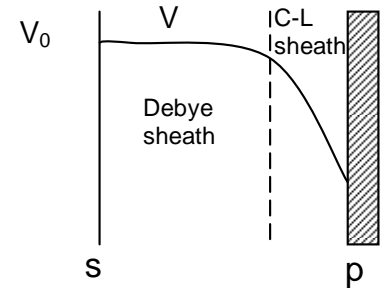


Fig. 1. Geometry of a plane sheath.

For Maxwellian electrons, we have

$$n_e = n_s e^{eV / KT_e}. \quad (3)$$

The ion velocity  $v$  is given by energy conservation

$$\frac{1}{2} M v_s^2 = \frac{1}{2} M v^2 + eV \quad (V \leq 0) \quad (4)$$

so that

$$v = \left( v_s^2 - \frac{2eV}{M} \right)^{1/2}. \quad (5)$$

Since ion flux is conserved, we have

$$n_i v_i = n_s v_s, \quad n_i = n_s v_s / v_i = n_s \left( 1 - \frac{2eV}{M v_s^2} \right)^{-1/2}. \quad (6)$$

The positive, dimensionless potential  $\eta$  is defined as

$$\eta \equiv -e(\tilde{V} - V_s) / KT_e = -eV / KT_e, \quad (7)$$

whereupon Poisson's equation becomes

$$\frac{\epsilon_0 KT_e}{n_s e^2} \frac{d^2 \eta}{dx^2} = \left( 1 + \frac{2KT_e}{M v_s^2} \eta \right)^{-1/2} - e^{-\eta}. \quad (8)$$

Henceforth we use a Roman "e" for charge and an italic "e" for 2.718. Normalizing  $x$  to the Debye length (with  $n = n_s$ ),

$$\lambda_D = \left( \epsilon_0 KT_e / n_s e^2 \right)^{1/2}; \quad \xi \equiv (x - s) / \lambda_D \quad (9)$$

and defining the ion acoustic speed  $c_s$  and the Mach number  $\mathcal{M}$  as

$$c_s \equiv (KT_e / M)^{1/2}, \quad \mathcal{M} \equiv v_s / c_s, \quad (10)$$

Eq. (8) becomes simply

$$\eta'' = \frac{d^2 \eta}{d\xi^2} = \left( 1 + 2\eta / \mathcal{M}^2 \right)^{-1/2} - e^{-\eta}. \quad (11)$$

Multiplying by the integrating factor  $\eta'$  and integrating from  $\xi = 0$ , we obtain

$$\frac{1}{2} (\eta')^2 = \mathcal{M}^2 \left[ \left( 1 + 2\eta / \mathcal{M}^2 \right)^{1/2} - 1 \right] + \left[ e^{-\eta} - 1 \right]. \quad (12)$$

Here we have used the sheath boundary condition  $\eta'(0) = 0$ .

## 2. Recovery of the Bohm sheath criterion

Since Eq. (12) has to be positive for all  $\eta$ , we can get a condition on  $\mathcal{M}$  by expanding the r.h.s. for small  $\eta$ , up to order  $\eta^2$ .

$$\begin{aligned} \frac{1}{2} (\eta')^2 &= \mathcal{M}^2 \left[ \left( 1 + \eta / \mathcal{M}^2 - \frac{1}{2} \eta^2 / \mathcal{M}^4 \right) - 1 \right] + \left[ 1 - \eta + \frac{1}{2} \eta^2 - 1 \right] \\ &= -\frac{1}{2} \eta^2 / \mathcal{M}^2 + \frac{1}{2} \eta^2 \geq 0. \end{aligned} \quad (13)$$

Hence,  $\mathcal{M} \geq 1$ , or  $v_s \geq c_s$ , which is the Bohm criterion. We can now *define* the “sheath edge” to be that position  $s$  near the wall or probe where this condition is barely satisfied:  $v_s = c_s$ . Setting  $\mathcal{M} = 1$  in Eq. (12) and taking the square root, we obtain

$$\eta' = \pm\sqrt{2} \left[ (1 + 2\eta)^{1/2} + e^{-\eta} - 2 \right]^{1/2}. \quad (14)$$

This equation differs from previous work on  $C_{\text{sh}}$  in that the electron density is not neglected or approximated.

### 3. Recovery of the Child-Langmuir law

For space-charge-limited ion emission, the electron terms are omitted, and  $\eta$  is infinitely large, since temperatures are zero. Eq. (14) then becomes

$$\eta' = 2^{1/2} (2\eta)^{1/4}, \quad \eta^{-1/4} \eta' = 2^{3/4}. \quad (15)$$

Integrating from  $\xi = 0$  to  $d / \lambda_D$  gives

$$\eta^{3/4} = \frac{3}{4} 2^{3/4} \xi_d, \quad \eta^{3/2} = \frac{9}{16} 2^{3/2} \xi_d^2 = \frac{9}{8} 2^{1/2} \xi_d^2. \quad (16)$$

Converting back to dimensional units, we have

$$\left( \frac{-eV}{KT_e} \right)^{3/2} = \frac{9}{8} 2^{1/2} d^2 \left( \frac{n_s e^2}{\epsilon_0 KT_e} \right). \quad (17)$$

It is now convenient to express  $n_s$  in terms of the ion current density  $J$ :

$$J = en_s c_s = en_s (KT_e / M)^{1/2}, \quad n_s = J / e(KT_e / M)^{1/2}. \quad (18)$$

The normalizing factor  $KT_e$  now cancels out, as it should, and we have

$$J = \frac{4}{9} \left( \frac{2e}{M} \right)^{1/2} \frac{\epsilon_0 (-V)^{3/2}}{d^2}, \quad (19)$$

which is exactly the Child-Langmuir law.

### 4. Relation to the plasma potential

Since the ions have a velocity  $c_s$  at  $s$ , they must have gained an energy  $\frac{1}{2} M c_s^2 = \frac{1}{2} K T_e$  in the presheath, so that the potential  $V_0$  in the main plasma must be higher than  $V_s$  by  $\frac{1}{2} K T_e / e$ . The electrons, if Maxwellian, would have a density higher by a factor  $e^{1/2}$  in the plasma than at the sheath edge. Thus,  $n_s = e^{-1/2} n_0 = 0.61 n_0$ . Since  $\lambda_D$  was defined with  $n_s^{-1/2}$ , its value would be decreased by  $e^{-1/4} = 0.78$  if we had chosen to define it using  $n_0$ . The derivative  $\eta'$  would be increased by a factor  $e^{1/4} = 1.28$ . However, once this is understood, it is not necessary to make any changes in the formulism.

### C. Calculation of sheath capacitance

The charge on a capacitor is given by  $Q = CV$ . From this, the sheath capacitance  $C_{\text{sh}}$  can be written as

$$\frac{C_{sh}}{A_p} = \frac{\Delta\rho_s}{\Delta V}, \quad (20)$$

where  $A_p$  is the probe area and  $\rho_s$  is the surface charge density on the probe. Following Ref. 6, we use Gauss's Law to obtain  $\rho_s = D_n$ , the normal component of  $\epsilon_0 E = -\epsilon_0(-\nabla V)$ . The first minus sign comes from the fact that  $D_n$  is defined in the  $-x$  direction in Fig. 1. Eq. (20) then becomes

$$\frac{C_{sh}}{A_p} = -\epsilon_0 \frac{\Delta E}{\Delta V} = \epsilon_0 \frac{d}{dV} \left( \frac{dV}{dx} \right) = \frac{\epsilon_0}{\lambda_D} \frac{d}{d\eta} \left( \frac{d\eta}{d\xi} \right). \quad (21)$$

Eq. (14) gives  $d\eta/d\xi$ . Taking its  $\eta$ -derivative, we obtain

$$\frac{C_{sh}}{A_p} = \frac{\epsilon_0}{\lambda_D} \frac{1}{\sqrt{2}} \frac{(1+2\eta)^{-1/2} - e^{-\eta}}{[(1+2\eta)^{1/2} + e^{-\eta} - 2]^{1/2}}, \quad (22)$$

where we have taken the  $+$  sign because the ion density (the first term in the numerator) has to be larger than the electron density (the second term) once the Bohm criterion is satisfied. Here it is understood that  $\eta$  is evaluated at the probe, so that  $\eta = -e(V_p - V_s)/KT_e$ . This equation is valid for all  $V_p$  below the space potential even if  $\eta$  is small.

The error in neglecting the Debye sheath<sup>6</sup> can now be calculated. With a large negative probe bias so that  $\eta \gg 1$ , the fraction  $F$  in Eq. (22) becomes

$$F = (1+2\eta)^{-1/2} [(1+2\eta)^{1/2} - 1]^{-1/2} = [(1+2\eta)^{3/2} - (1+2\eta)]^{-1/2}. \quad (23)$$

This can be expanded in the small quantity  $\epsilon \equiv 1/(2\eta)$  to obtain

$$F = \epsilon^{3/4} \left( 1 - \epsilon^{1/2} + \frac{3}{2}\epsilon - \dots \right)^{-1/2} \approx \epsilon^{3/4} \left( 1 + \frac{1}{2}\epsilon^{1/2} - \frac{3}{4}\epsilon + \dots \right). \quad (24)$$

Thus the capacitance is approximately

$$\frac{C_{sh}}{A_p} = \frac{\epsilon_0}{\lambda_D} \frac{(2\eta)^{-3/4}}{2^{1/2}} \left( 1 + \frac{1}{2} \frac{1}{(2\eta)^{1/2}} \right). \quad (25)$$

Apart from notation, this is the same as Eq. (17) of Ref. 6 if one approximates  $n_s$  with  $\frac{1}{2}n_0$  (Sec. A4). The correction term in Eq. (25), which modifies the Child-Langmuir sheath for the incident ion velocity, is not small. At the floating potential,  $\eta$  is about 5, so that term is  $\approx 0.16$ . For smaller  $\eta$  ( $V_p$  closer to space potential) the expansion fails, and one should use the exact equation (22), which includes the Debye sheath. Physically, Eq. (25) tells us that the sheath capacitance increases as  $\eta$  decreases—that is, as the sheath gets thinner—more or less as predicted by the Child-Langmuir law. There is, in addition, a dependence on  $T_e$  and  $n_0$  through  $\lambda_D$ .

Figure 2 shows computations of  $C_{sh}$  vs.  $\eta$  comparing the exact formula of Eq. (22) with the approximate formulas of Eqs. (25) and (28). At large  $\eta$ , all the curves show a decrease of  $C_{sh}$  with  $\eta$  as the C-L sheath thickness increases. The exact curve shows a peak at small  $\eta$  as the probe enters the Debye sheath, and it falls at smaller  $\eta$  as the thickness of the Debye sheath increases to  $\infty$  as  $V_p$  reaches the space potential. Approximations that do not include the Debye sheath do not have this feature. The approximation (25) that includes the ion velocity at the sheath edge is somewhat better than the C-L approximation (28), which does not. The improve-

ment is not great, since the series in Eq. (24) converges very slowly with  $\eta^{-1/2}$ . At the floating potential either approximation is reasonably good, but they fail when the  $V_p$  moves closer to  $V_s$ . Figure 3 shows the expected variation of  $C_{sh}$  with density.

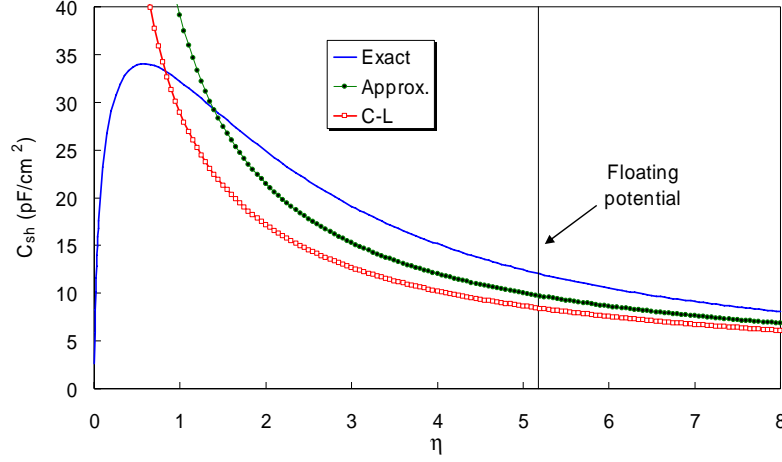


Fig. 2. Sheath capacitance vs. normalized probe bias according to the exact formula (—), its Taylor expansion (●), and the Child-Langmuir formula (○).

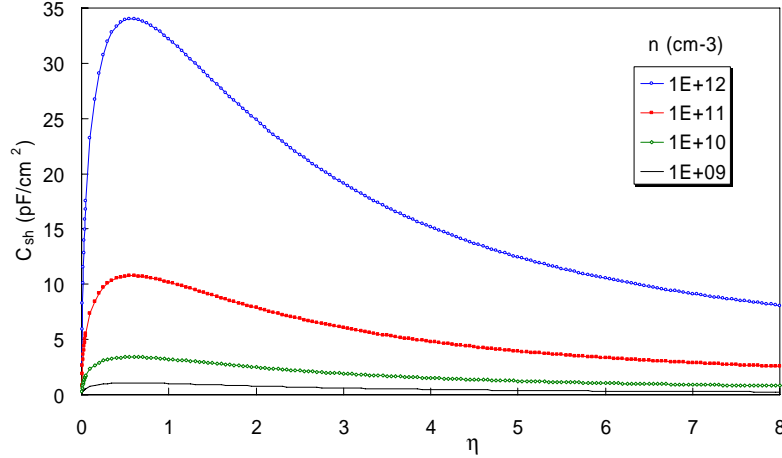


Fig. 3. Variation of dc  $C_{sh}$  with density.

## D. Effect of RF

### 1. Range of validity

In rf discharges, an electric field is applied to the plasma either by an electrode or by an external antenna. This E-field can drive electrons towards a wall. The sheath drop there must then increase to repel enough electrons to maintain a neutral plasma, and the plasma potential  $V_0$  must rise. As the rf changes sign,  $V_0$  will rise and fall unsymmetrically, since the current through a Coulomb barrier varies exponentially with voltage. The harmonic content of  $V_0$  oscillations will vary in different devices. Godyak and Piejak<sup>7</sup> showed that the 2nd harmonic will dominate in a CCP with electrodes driven symmetrically relative to ground<sup>4</sup>. In a normal CCP with one electrode near ground, the fundamental rf frequency  $\omega$  will dominate. In a cylindrical inductively coupled plasma (ICP), the E-field is ideally everywhere parallel to the walls, so that no oscillating wall sheaths develop, but asymmetries in antenna construction, ports on the walls, and

capacitive coupling can cause  $V_0$  oscillations at the fundamental frequency  $\omega$ . In helicon discharges, an E-field at  $\omega$  is an intrinsic property of the helicon wave. To simplify the problem, we will treat one frequency at a time and assume that  $V_s$ , the sheath-edge potential, follows the oscillations in  $V_0$ .

The dc sheath theory given above is applicable only if the sheath comes into equilibrium at each phase of the rf. This requires, first, that the rf frequency  $f_{rf}$  be low enough that the electrons respond instantaneously; this is a good assumption. Second, the frequency must be low enough that the ions traverse the sheath before it changes, and their rf motion need not be taken into account<sup>3,5</sup>. If the sheath thickness is about  $5\lambda_D$ , the ion transit time  $t$  through the sheath is

$$t \approx 5\lambda_D / c_s \approx 5 \left( \frac{\epsilon_0 K T_e}{n_0 e^2} \right)^{1/2} \left( \frac{M}{K T_e} \right)^{1/2} = \frac{5}{\Omega_p}, \quad (26)$$

$\Omega_p$  being the ion plasma frequency. The rf period  $\tau = 1/f_{rf} =$  must then be  $\gg 2t$ , yielding

$$f_{rf} \ll \Omega_p / 10. \quad (27)$$

At  $n_0 = 10^{12} \text{ cm}^{-3}$ ,  $\Omega_p$  is  $\approx 2 \times 10^8 \text{ sec}^{-1}$ , so that  $f_{rf}$  must be  $\ll 20 \text{ MHz}$ . This is marginally acceptable at 13.56 MHz, and the condition is not met at lower densities even at that frequency. Fortunately, the value of  $C_{sh}$  need not be known exactly in practical applications.

This being the case, we may use Eq. (25) without the correction term; the error entailed was discussed in Sec. C. In dimensional units, this is

$$C_{sh} = \frac{A_p}{2^{5/4}} \frac{\epsilon_0}{\lambda_D} \left[ \frac{e(V_s - V_p)}{K T_e} \right]^{-3/4}. \quad (28)$$

In the absence of rf, the capacitance is<sup>6</sup>

$$C_0 = \frac{A_p}{2^{5/4}} \frac{\epsilon_0}{\lambda_D} \left[ \frac{e(\bar{V}_s - \bar{V}_p)}{K T_e} \right]^{-3/4}, \quad (29)$$

where the overbar denotes the dc values.

## 2. Uncompensated probe

**a) Small rf fluctuations.** In the presence of rf, consider first a probe or small electrode connected directly to a dc power supply, giving  $V_p = \bar{V}_p$ . Let  $V_s$  oscillate at frequency  $\omega$

$$V_s = \bar{V}_s + V_{rf} \sin \omega t. \quad (30)$$

The capacitance is then given by

$$C_{sh} = C_0 \left( 1 + \frac{V_{rf} \sin \omega t}{\bar{V}_s - \bar{V}_p} \right)^{-3/4}. \quad (31)$$

In addition to  $C_{sh}$  changing with probe voltage, it also changes during an rf cycle. If  $V_{rf}$  is small, Eq. (31) can be expanded and averaged over an rf cycle. We then find that  $\langle C_{sh} \rangle$  differs from  $C_0$  only in second order in  $V_{rf} / (\bar{V}_s - \bar{V}_p)$ .



**b) Large rf fluctuations.** A more likely situation, however, is that  $V_{rf}$  is larger than  $\bar{V}_s - \bar{V}_p$ , which can be as small as  $2KT_e/e$  as the probe  $I - V$  curve is swept, while  $V_{rf}$  can exceed 100V. In that case, Eq. (31) shows that  $C_{sh}$  has a pole and becomes complex when the bracketed quantity goes negative. This cannot happen physically, however. When  $V_s$  comes close to  $V_p$ , a the probe draws a large electron current, raising the mean plasma potential  $\bar{V}_s$ . Thus,  $\bar{V}_s$  has to increase, keeping the bracket positive. Since  $\bar{V}_s$  is no longer constant and the approximation  $\eta \gg 1$  is not always valid, we must use the exact equation (22):

$$\frac{C_{sh}}{A_p} = \frac{\epsilon_0}{\lambda_D} \frac{1}{\sqrt{2}} \frac{(1+2\eta)^{-1/2} - e^{-\eta}}{\left[(1+2\eta)^{1/2} + e^{-\eta} - 2\right]^{1/2}}. \quad (32)$$

Under normal circumstances,  $\eta$  is always positive if the probe is biased below  $V_s$ . The denominator is positive if the Bohm criterion is satisfied (Sec. B2), and the numerator is always positive since its leading term in a Taylor expansion is  $\eta^2$ . Recall that  $\eta$  is defined as

$$\eta = \frac{e}{KT_e} \left[ V_{rf} \sin \omega t + (\bar{V}_s - \bar{V}_p) \right]. \quad (33)$$

If  $\sin \omega t$  is positive or only slightly negative so that  $\eta$  remains positive, electron saturation is never reached, and Eq. (32) is still correct. For more negative values of  $\sin \omega t$ ,  $\eta$  would become negative unless  $\bar{V}_s$  increases. The amount of this increase depends on the geometry. To keep the plasma neutral, the electron flux to the probe cannot exceed the ion flux to the walls. For simplicity, we neglect the ion flux to the probe and the electron flux to the walls. The electron flux to the probe is

$$J_e = A_p n_0 v_r e^{-\eta} \quad (\eta \geq 0), \quad v_r = (KT_e / 2\pi m)^{1/2}, \quad (34)$$

where  $v_r$  is the electrons' random thermal velocity. The ion flux to the walls of area  $A_w$  is

$$J_i = A_w n_s c_s = A_w e^{-1/2} n_0 (KT_e / M)^{1/2}. \quad (35)$$

The minimum value of  $\eta$  is thus given by equating these two fluxes:

$$e^{\eta_{\min}} = \frac{A_p n_0 v_r}{A_w n_s c_s} = \frac{A_p}{A_w} \left( \frac{e}{2\pi} \frac{KT_e}{m} \frac{M}{KT_e} \right)^{1/2}, \quad (36)$$

$$\eta_{\min} = \frac{1}{2} \left[ 1 + \ln \left( \frac{M}{2\pi m} \frac{A_p^2}{A_w^2} \right) \right]. \quad (37)$$

Note that “ $e$ ” here is *not* the unit charge “ $e$ ”. From Eq. (33),  $\bar{V}_s$  must rise to the value

$$\bar{V}_s = \bar{V}_p - V_{rf} \sin \omega t - (KT_e / e) \eta_{\min}. \quad (38)$$

For rf phases such that  $\sin \omega t$  is negative and large enough that  $\eta < \eta_{\min}$  in Eq. (33), the sheath capacitance is given by Eq. (32) with  $\eta$  replaced by  $\eta_{\min}$ . Thus, for large  $V_{rf}$ ,  $C_{sh}$  obeys Eq. (32) for only part of the rf cycle. When  $\sin \omega t$  swings sufficiently negative,  $\bar{V}_s$  rises to keep the plasma neutral, and  $C_{sh}$  remains constant during that part of the rf cycle.

Note, however, that Eq. (34) is valid only for  $\eta \geq 0$ . Electron saturation is reached at  $\eta = 0$ , and  $J_e$  remains at the value  $A_p n_0 v_r$ . That means that  $\eta_{\min}$  must be non-negative and the argument of the logarithm in Eq. (37) must be  $> 1/e$ . If the probe area is so small that it can draw saturation electron current without raising  $V_s$ , then the sheath vanishes, having infinite thickness. Indeed, if we replace  $\eta$  by  $\eta_{\min} = 0$  in Eq. (32), we find that  $C_{\text{sh}}$  has the indeterminate form  $0/0$ , which can be seen to approach 0 by taking the derivatives of the numerator and denominator.

In summary, we see that  $C_{\text{sh}}$  varies in a very complicated way in the presence of  $V_{\text{rf}}$ . There are four cases: i) If  $V_{\text{rf}}$  is so small that  $V_s$  never oscillates below  $\bar{V}_p$ ,  $C_{\text{sh}}$  is affected only in higher order. ii) For larger  $V_{\text{rf}}$ ,  $C_{\text{sh}}$  will vary nonsinusoidally with the phase of the rf. iii) If  $V_{\text{rf}}$  is very large,  $\bar{V}_s$  will be changed by the probe current so as to keep  $\eta$  positive, and  $C_{\text{sh}}$  will reach a limiting value during part of the rf cycle. iv) If the probe is very small,  $\eta_{\min}$  itself will saturate at the value 0. These cases are illustrated in Figs. 4–6. Figure 4 compares  $C_{\text{sh}}$  computed using Eq. (32) with that using Eq. (31). At  $V_{\text{rf}} = 6\text{V}$ , the excursions are small enough that  $\eta$  does not enter the region to the left of the peak in Fig. 2, and is near the limit of case (i). At  $V_{\text{rf}} = 8\text{V}$ , that region is entered when  $\sin\omega t \approx -1$ , and the exact solution shows a dip in  $C_{\text{sh}}$ . This dip reaches 0 at  $V_{\text{rf}} = 9\text{V}$ , since  $e(V_s - V_p)$  starts at  $3KT_e = 9\text{V}$ , and  $V_{\text{rf}}$  is just sufficient to bring  $V_s$  down to  $V_p$  at its extremum. This is case (ii).

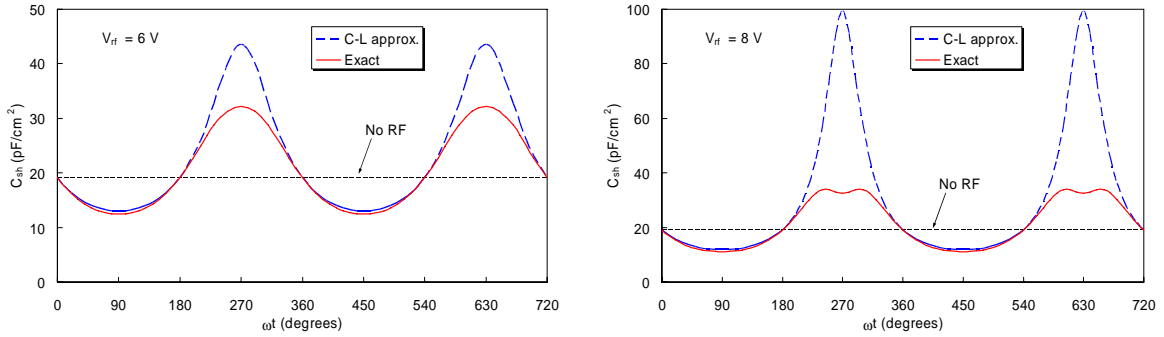


Fig. 4. Variation of  $C_{\text{sh}}$  through two rf cycles for  $V_{\text{rf}} = 6$  and  $8\text{V}$  (0-to-peak). The solid curve (—) is the exact solution, and the dashed curve (- - -) the C-L approximation. Parameters are  $n = 10^{12}\text{ cm}^{-3}$ ,  $KT_e = 3\text{ eV}$ , and  $\eta_{\text{dc}} = 3$ .

Figure 5 shows case (iii), when  $\eta$  is limited by  $\eta_{\min}$ , but  $\eta_{\min}$  is still above the dc value of  $\eta = 3$ . The “exact” solution of Eq. (32) is compared with that when the  $\eta_{\min}$  cutoff is imposed by the fact that  $V_s$  is dragged upward by the probe current. This rare case happens only when the plasma chamber is small, so that the ratio  $A_w/A_p$  in Eq. (37) is not very large. However, we have observed experimentally that the shift is  $\bar{V}_s$  is larger than expected from the calculation above, so that case (iii) may occur for larger values of  $A_w/A_p$ .

### 3. Partially compensated probe

The most common way to deal with rf fluctuations in  $V_0$  is to use tuned inductors and auxiliary floating electrodes, a method tried by Gagne and Cantin<sup>8,9</sup> and further developed by Godyak et al.<sup>10</sup>, Sudit and Chen<sup>6</sup>, and Mahony et al.<sup>11</sup> A partially compensated probe is shown in Fig. 7. The probe tip is located at P. The sheath capacitance  $C_{sh}$  connects it to the space potential  $V_s$ . A choke chain with impedance  $Z_{ck}$  consisting of inductors and their stray capacitances filters out the rf fluctuations  $\tilde{V}_s$  from the resistor  $R_m$  across which the probe current is measured. The value of  $R_m$  is small and can be neglected in this discussion. Ideally, the probe tip then fluctuates with  $\tilde{V}_s$  so that the applied dc voltage  $V_p$  is the only voltage between the probe and the plasma. Ignoring the stray capacitance  $C_s$  for the moment, we see that  $C_{sh}$  and  $Z_{ck}$  form a voltage divider, and the rf signal at P is

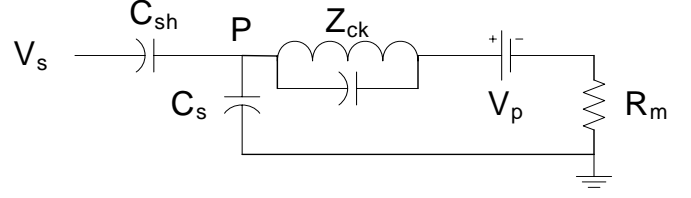


Fig. 7. Isolation of a probe with a choke.

$$\tilde{V}_p = \tilde{V}_s \frac{Z_{ck}}{Z_{ck} + Z_{sh}}, \quad (39)$$

where  $Z_{sh}$  is  $-j/\omega C_{sh}$ . To suppress rf pickup, therefore,  $|Z_{ck}|$  must be much larger than  $|Z_{sh}|$  so that  $\tilde{V}_p$  follows  $\tilde{V}_s$  closely. To get probe  $I - V$  characteristics unaffected by  $\tilde{V}_s$  requires

$$\eta_{rf} = (e/KT_e)(\tilde{V}_s - \tilde{V}_p) \ll 1, \quad (40)$$

where

$$\eta = \eta_{dc} + \eta_{rf} = (e/KT_e)(\bar{V}_s + \tilde{V}_s - \bar{V}_p - \tilde{V}_p). \quad (41)$$

From Eq. (39) with  $\tilde{V}_s \approx \tilde{V}_{rf}$ , the requirement is<sup>7</sup>

$$\frac{e\tilde{V}_{rf}}{KT_e} \left| \frac{Z_{sh}}{Z_{ck} + Z_{sh}} \right| \approx \frac{e\tilde{V}_{rf}}{KT_e} \left| \frac{Z_{sh}}{Z_{ck}} \right| \ll 1. \quad (42)$$

To get an order of magnitude, we can use Eq. (29) to estimate  $C_{sh}$ . For typical parameters  $A_p = .047 \text{ cm}^2$  (0.15 mm diam  $\times$  1 cm long),  $KT_e = 3 \text{ eV}$ ,  $n = 10^{12} \text{ cm}^{-3}$ , this gives  $C_0 = 42 \text{ pF}$  and  $|Z_{sh}| = 280 \Omega$  at 13.56 MHz. Here we have assumed  $\bar{V}_p$  near floating potential, so that  $\bar{V}_p - \bar{V}_s \approx 5$ . If  $\tilde{V}_{rf} = 100\text{V}$ , we would require  $|Z_{ck}| \gg 10 \text{ k}\Omega$ , or  $|Z_{ck}| \geq 100 \text{ k}\Omega$ . At lower densities, this value increases as  $n^{-1/2}$ . To get an impedance this high usually requires using tuned chokes whose self-resonance is at the rf frequency.

### 4. Fully compensated probe

A choke chain alone, however, is insufficient because of the stray capacitance  $C_s$  of the short wire between the probe tip and the choke chain<sup>7,6</sup>. If  $C_s$  connects P to ground, it effectively decreases the value of  $|Z_{sh}|$ . If  $C_s$  connects P to the plasma through a ceramic probe insulator, it has little effect, since it simply adds a small amount to  $C_{sh}$ . If  $\tilde{V}_s$  varies in space, there may be a small difference between the  $\tilde{V}_s$  sampled by  $C_s$  and that seen by the probe tip, but this cannot be a large effect.

However, in a real situation, it was found<sup>6</sup> that  $|Z_c| \approx 200\text{k}\Omega$  gave insufficient rf isolation even if a metal probe shaft was not used. In this case, an auxiliary electrode or “compensation electrode” of large area  $A_x$  (and hence large  $C_x$ ), is required to detect the rf changes in  $V_0$ . Figure 8 shows the probe circuit with both sheaths included<sup>6</sup>. Here  $C_{sh}$  is on the probe tip and  $C_x$  is on the auxiliary electrode. The latter is coupled to the probe through the relatively large capacitor  $C_{cp}$ .  $C_x$  is given by Eqs. (32) and (33) but with a larger area  $A_x$ , large enough to satisfy Eq. (42) even if  $Z_{ck}$  is bypassed by the stray capacitance  $C_{s1}$ .

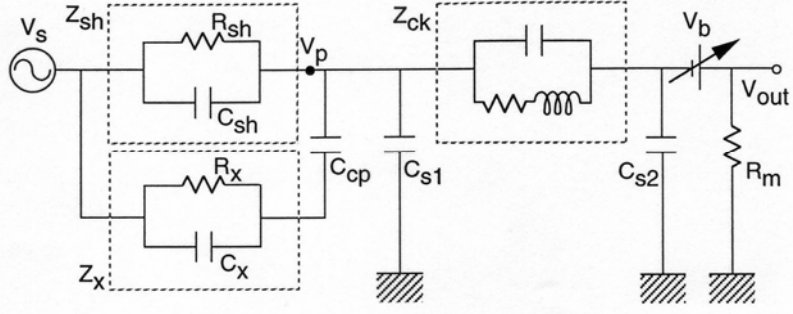


Fig. 8. Equivalent circuit of a compensated probe (from Ref. 1).

As far as the probe is concerned,  $\tilde{V}_p$  is driven by the compensation electrode and is given by Eq. (39) with  $Z_x$  in place of  $Z_{sh}$ :

$$\tilde{V}_p = \tilde{V}_s \left| \frac{Z_{ck}}{Z_{ck} + Z_x} \right|. \quad (43)$$

The requirement of Eq. (42) is then relaxed to

$$\frac{e\tilde{V}_{rf}}{KT_e} \left| \frac{Z_x}{Z_{ck} + Z_x} \right| \approx \frac{e\tilde{V}_{rf}}{KT_e} \left| \frac{Z_x}{Z_{ck}} \right| \ll 1, \quad (44)$$

and  $|Z_{ck}|$  can be smaller by the ratio  $A_x / A_p$ . If  $A_x$  is large enough, it may not be necessary to use resonant chokes. For instance, if  $A_p \approx .05 \text{ cm}^2$ , and  $A_x \approx 5 \text{ cm}^2$  (0.5 cm diam  $\times$  3 cm long),  $|Z_{ck}|$  can be reduced a factor 100 below the 100 k $\Omega$  calculated in the previous example. However, note that  $C_{sh}$  depends on  $1/\lambda_D \propto \sqrt{n}$ . If  $n \approx 10^9 \text{ cm}^{-3}$  instead of  $10^{12} \text{ cm}^{-3}$ ,  $|Z_{sh}|$  is increased by a factor of 32, and  $|Z_{ck}|$  of order 30 k $\Omega$  is still required.

## 5. Generation of harmonics

Since  $C_{sh}$  varies with  $V_s$ , the rf probe current will be non-sinusoidal, and harmonics of the rf frequency will be generated. To estimate this, we use the approximate formula (31):

$$C_{sh} = C_0 \left( 1 + \frac{V_{rf} \sin \omega t}{\bar{V}_s - \bar{V}_p} \right)^{-3/4}. \quad (45)$$

The ac electron current to the probe is given by

$$\tilde{I}_e = C_{sh} (dV_s / dt). \quad (46)$$

From Eqs. (30) and (45), we obtain

$$\tilde{I}_e = C_0 \left( 1 + \frac{V_{rf} \sin \omega t}{\bar{V}_s - \bar{V}_p} \right)^{-3/4} (V_{rf} \omega \cos \omega t). \quad (47)$$

For sufficiently small  $V_{rf}$ , Taylor expansion gives

$$\tilde{I}_e = C_0 \left( 1 - \frac{3}{4} \frac{V_{rf} \sin \omega t}{\bar{V}_s - \bar{V}_p} \right) (V_{rf} \omega \cos \omega t) = \omega C_0 V_{rf} \left( \cos \omega t - \frac{3}{8} \frac{V_{rf} \sin 2\omega t}{\bar{V}_s - \bar{V}_p} \right). \quad (48)$$

When the expansion is valid, the 2nd harmonic is smaller than the fundamental by a factor<sup>6</sup>

$$\frac{3}{8} \frac{V_{rf}}{\bar{V}_s - \bar{V}_p}. \quad (49)$$

This is, of course, valid only for very small values of  $V_{rf}$ . To see the effect of a more exact calculation, we have Fourier analyzed the fairly smooth curve of Fig. 4b, representing a  $V_{rf}$  of only 8V. The Fourier fit up to the 8th harmonic are shown in Fig. 9. The non-zero coefficients  $a_n$  of  $\sin(n\omega t)$  and  $b_n$  of  $\cos(n\omega t)$  are given relative to that of the fundamental,  $a_1$ . The largest harmonic, the 2nd, has 13% amplitude in this case. The leading term in  $\tilde{I}_e$  is still given by Eq. (48).

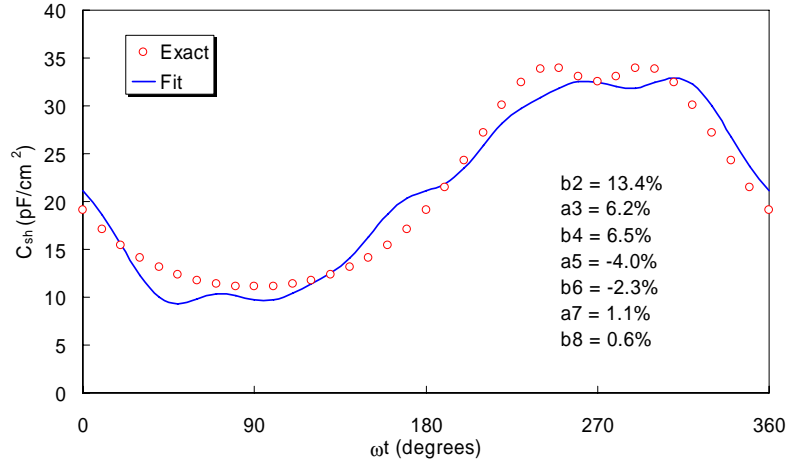


Fig. 9. A Fourier fit to the exact curve of Fig. 4 for  $V_{rf} = 8V$ . The harmonic amplitudes relative to the fundamental are shown.

## 6. The sheath resistance

The real part of  $Z_{sh}$ , corresponding to the particle current to the probe, is also nonlinear. We consider only the electron current, since the ion current is comparatively constant and is not greatly changed by fluctuations in  $V_s$ . For a Maxwellian distribution the electron current is given by Eq. (34):

$$I_e = -eA_p n_0 v_r e^{(V_s - V_p)/KT_e}. \quad (50)$$

The sheath resistance is defined by

$$R_{sh} = dV / dI, \quad (51)$$

so that, in the absence of rf, the dc resistance is given by

$$R_{sh}^{-1} = dI_e / d(V_p) = (e / KT_e) |I_e|, \quad (52)$$

with  $V_s = \bar{V}_s = \text{constant}$ . At the floating potential,  $|I_e|$  is equal to  $I_i$ , and  $R_{sh}$  there is given by

$$R_{sh}(V_f) = \frac{KT_e}{e} \frac{1}{eI_i} = \frac{KT_e}{e^2} \frac{1}{n_s c_s A_p} = \frac{KT_e}{e^2} \frac{1}{e^{-1/2} n_0 c_s A_p} = \frac{(eMKT_e)^{1/2}}{A_p n_0 e^2}. \quad (53)$$

Note that the “ $e$ ” in italics is not the unit charge. As the probe bias  $\bar{V}_p$  increases,  $|I_e|$  increases, and  $R_{sh}$  decreases from this value exponentially.

In the presence of rf,  $V_s$  will oscillate and be given by  $V_s = \bar{V}_s + V_{rf} \sin \omega t$ . If the probe is uncompensated,  $V_p$  will remain at  $\bar{V}_p$ . The  $I - V$  curve will oscillate horizontally, and its slope will change, causing  $R_{sh}$  to change nonlinearly during the rf cycle. Its value is still given by Eqs. (52) and (50) if  $V_s$  is given its unsteady value. If the probe is rf compensated, as Sec. D4,  $V_p$  will follow  $V_s$ , and the slope of the  $I - V$  curve will not change as much.  $R_{sh}$  is still given by Eqs. (52) and (50) if  $V_s - V_p$  is given its compensated value. From Eq. (43) we obtain

$$\tilde{V}_s - \tilde{V}_p = V_{rf} \sin \omega t \left| \frac{Z_x}{Z_{ch} + Z_x} \right|. \quad (54)$$

The instantaneous sheath resistance from Eqs. (52), (50), and (54) can now be written

$$R_{sh} = \frac{KT_e}{e} e^{-\left[ \bar{V}_s - \bar{V}_p + \frac{e}{KT_e} \left| \frac{Z_x}{Z_{ch} + Z_x} \right| V_{rf} \sin \omega t \right]}. \quad (55)$$

The same proviso on negative values of  $\sin \omega t$  that make the exponent positive applies here, but with good compensation this should not happen. The dynamic impedance of a plane sheath in a strong rf environment is then given by

$$Z_{sh} = R_{ch} - j / \omega C_{sh}, \quad (56)$$

in which the resistive and reactive elements have been treated in detail above.

## E. Cylindrical geometry

A compensation electrode is usually large enough compared with  $\lambda_D$  that the sheath on it can be treated as planar. A wire probe tip, however, is likely to be made with radius  $R_p$  smaller than or comparable to  $\lambda_D$  in order for the orbital-motion-limited probe theory to be applicable. In that case, the probe sheath has to be treated in cylindrical geometry. In the electron retardation region, Poisson's equation (11) is replaced by the cylindrical version<sup>12</sup> of the Allen-Boyd-Reynolds<sup>13</sup> (ABR) equation

$$\frac{1}{\rho} \frac{d}{d\rho} \left( \rho \frac{d\eta}{d\rho} \right) = \frac{J}{\rho} \eta^{-1/2} - e^{-\eta}, \quad J \equiv \frac{1}{2\pi\sqrt{2}} \frac{I_i}{en_0} \frac{1}{\lambda_D c_s}, \quad (57)$$

where  $\rho = r / \lambda_D$ . This equation is not amenable to an analytic solution suitable for probe design. It has to be integrated from infinity, and it does not make sense<sup>14</sup> to define a sheath edge where  $v_i = c_s$ . Furthermore, the ion current  $I_i$  has to be assumed at the outset.

Although we cannot easily extend the plane results for the retardation region to cylinders, we can treat the region of electron saturation. When  $V_p > V_s$  so that  $\eta < 0$ , electrons are accelerated toward the probe. Their thermal velocities will cause those with high angular momentum to

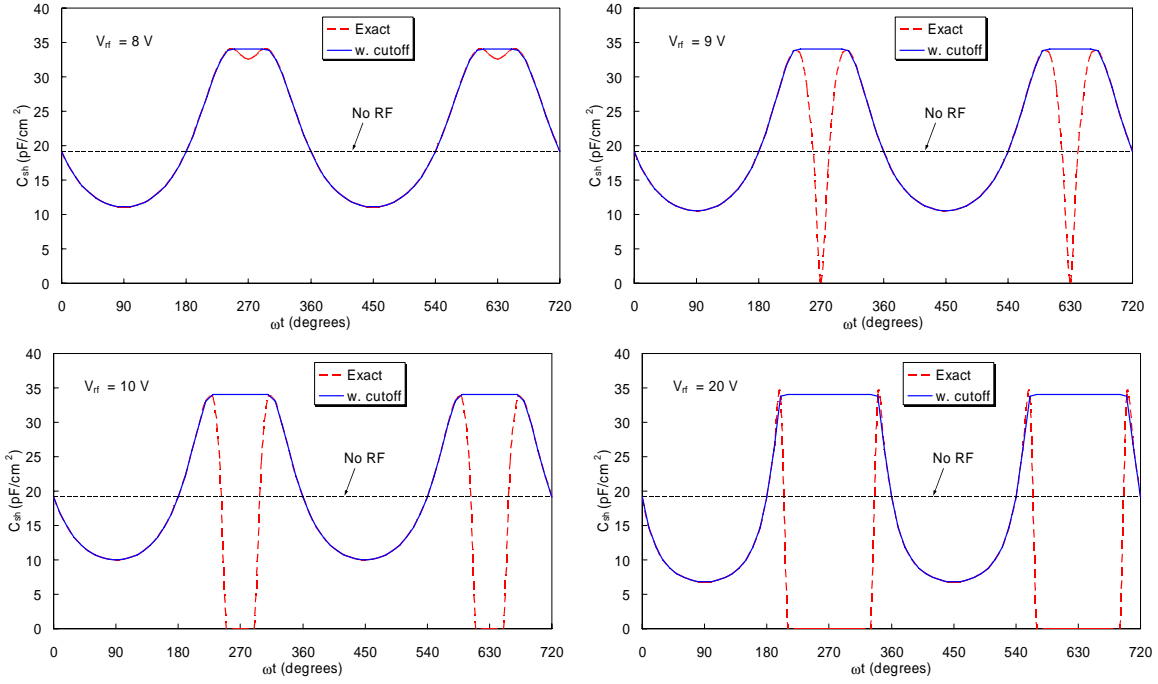


Fig. 5. Comparison of the “exact” solution (---) with that imposed by  $\eta_{\min}$  as  $V_{\text{rf}}$  is increased (—). The  $V_{\text{rf}} = 8\text{V}$  case is the same as in Fig. 4. The ratio  $A_w/A_p$  is only 100 here.

Figure 6 shows case (iv) when  $A_w/A_p$  has a more normal value of  $2800/0.047$  (an  $0.015 \times 1$  cm diam probe in a  $30\text{-cm}$  diam  $\times 30$  cm high chamber). In this case, the large  $V_s$  oscillations quickly bring  $V_s$  down to  $V_p$  whenever  $\sin\omega t$  is negative, and  $\eta_{\min} \rightarrow 0$  for a large portion of the rf period.  $C_{\text{sh}}$  also goes to 0, corresponding to the left edge of the exact curve in Fig. 2. The only difference between the curves is that the “exact” equation (32) has no solution for  $\eta < 0$ , while “cutoff” solution replaces  $\eta$  with  $\eta_{\min} = 0$ .

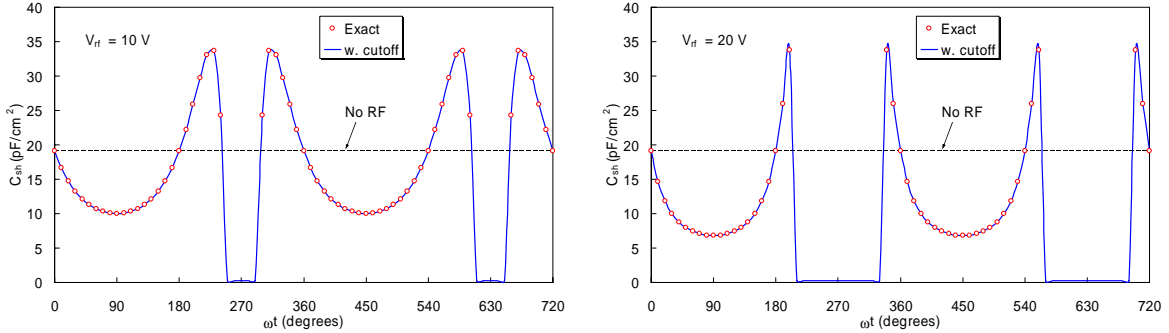


Fig. 6. Behavior of  $C_{\text{sh}}$  for small probes and large  $V_{\text{rf}}$ . The “exact” solution (○) does not exist where the “cutoff” solution (—) gives  $C_{\text{sh}} = 0$ .

The sudden jumps in  $C_{\text{sh}}$  would give rise to high harmonics in the probe current. These jumps are an artifact of the plane-geometry idealization. In cylindrical geometry the electron current does not saturate abruptly but slowly grows as the electron sheath expands. The curves in Fig. 6 should be smoothed out, but we shall see in Sec. E that the situation is not simple. In the next two sections, we examine methods devised to avoid the complicated behavior of  $C_{\text{sh}}$  by limiting the effective  $V_{\text{rf}}$  to small values.

orbit the probe and miss it; they cannot be treated as a cold fluid, as we did with the ions. The equations have been solved numerically by Laframboise<sup>15</sup>, but these specific results cannot be applied to the general case. However, if  $R_p / \lambda_D$  is small enough, it is possible to use the convenient Orbital-Motion-Limited (OML) theory of Mott-Smith and Langmuir<sup>16</sup>, as summarized by Chen<sup>17</sup>. The orbits of particles spiraling in to an attractive probe are calculated using energy and momentum conservation as in Sec. B1, but in the case of electrons one cannot neglect their energy spread at the sheath edge. For a Maxwellian distribution at  $r = s$ , the OML result for saturation electron current is

$$I_{e,sat} = A_p e n_0 v_r F, \quad (58)$$

where  $v_r$  is given by Eq. (34), and  $F$  is the function

$$F \equiv \frac{1}{\varepsilon} \operatorname{erf}(\Phi^{1/2}) + e^{-\eta} [1 - \operatorname{erf}(\Phi - \eta)^{1/2}], \quad (59)$$

in which

$$\varepsilon \equiv R_p / s < 1, \quad \Phi \equiv \eta / (1 - \varepsilon^{-2}), \quad \Phi - \eta = \eta / (\varepsilon^2 - 1). \quad (60)$$

Here  $\eta$  is still defined by Eq. (7) and is negative for  $V_p > V_s$ , so that the arguments of the error functions

$$\operatorname{erf}(x) \equiv \int_0^x e^{-t^2} dt \xrightarrow{x \rightarrow 0} \frac{2x}{\sqrt{\pi}} \quad (61)$$

are real. The sheath radius  $s$  has to be arbitrarily assumed, since there is no Bohm criterion for electrons when  $T_e > T_i$ . However, it turns out that  $F$  is extremely insensitive to  $\varepsilon$  for all  $\varepsilon > 10$ , a fact that Langmuir could not point out because he did not have personal computers. We may therefore take the  $s \rightarrow \infty$  limit of Eq. (59), obtaining

$$F(\eta) = \frac{2}{\sqrt{\pi}} (-\eta)^{1/2} + e^{-\eta} [1 - \operatorname{erf}(-\eta)^{1/2}]. \quad (62)$$

Note that at the space potential  $\eta = 0$ ,  $F \rightarrow 1$  and  $F'(\eta) \rightarrow -1$ , so that  $I_{e,sat}$  joins smoothly onto the transition region [Eq. (34)]. An ideal OML probe curve is shown in Fig. 10. At  $V_s = 0$ , the junction at  $V_s$  is smooth for a cylindrical probe but abrupt for a plane probe. As  $V_{rf}$  oscillates with amplitude 6V, the probe bias  $V_p$  effectively oscillates relative to this curve between the limits shown. In this case,  $V_{rf}$  is large enough that the probe enters the electron saturation region during part of the rf cycle, but  $I_e$  does not change discontinuously, as it does in the plane case.

Eqs. (58) and (62) give  $I_e$  without the need for solution of Poisson's equation to get  $V(r)$ . Whether a collisionless electron coming from infinity hits the probe or not depends only on its initial energy and angular momentum regardless of the shape of  $V(r)$ . The requirement  $R_p \ll \lambda_D$  stems from the fact that  $n$  has to be small enough that there is no absorption radius  $R_a$  inside of which all electrons are collected, thus increasing the effective probe radius from  $R_p$  to  $R_a$ . To calculate  $C_{sh}$ , however, Eq. (21) requires a knowledge of  $\eta(\rho)$ , which is not available from the OML theory. Note, however, that the solution given by Eqs. (58) and (62) is self-similar; the



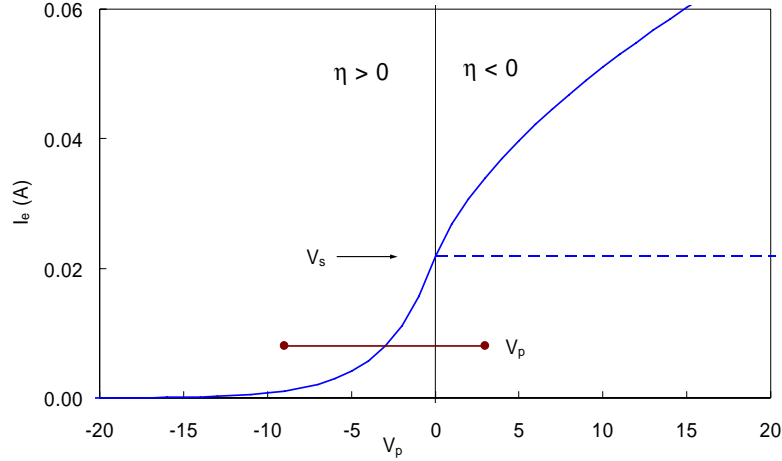


Fig. 10. An ideal OML curve for a cylindrical probe with  $R_p = .0075$  and  $L = 1$  cm. The argon plasma has  $KT_e = 3\text{eV}$  and  $n = 10^{11} \text{ cm}^{-3}$ . The dashed line is the saturation electron current for a plane probe. The effective excursion of  $V_p$  is shown for  $V_{rf} = 6\text{V}$  and  $\eta_0 = 1$ .

only scalelength is given by  $R_p$ . The ratio  $I_e / R_p$  depends only on  $\eta$ . Thus, as  $R_p$  changes, the picture is the same, and only the scale changes. All the particle trajectories have the same shape, and therefore the surface charge density  $\rho_s$  is proportional to  $I_e / R_p$ , and hence to  $F(\eta)$ . Let

$$\rho_s = \tau_1 (I_e / A_p), \quad (63)$$

where  $\tau_1$  is a constant with the dimensions of time. Eqs. (20), (58), and (63) then give

$$\frac{C_{sh}}{A_p} = \frac{d\rho_s}{dV} = -\frac{e}{KT_e} \frac{d}{d\eta} (\tau_1 n_0 e v_r F). \quad (64)$$

With Eqs. (9) and (34), this can be written

$$\frac{C_{sh}}{A_p} = -\frac{1}{\sqrt{2\pi}} \frac{\epsilon_0}{\lambda_D} \omega_p \tau_1 F'(\eta). \quad (65)$$

Differentiating Eq. (62) gives

$$F'(\eta) = -e^{-\eta} \{1 - \text{erf}[(-\eta)^{1/2}]\}, \quad (66)$$

where  $\eta$  is negative. The sheath capacitance in electron saturation is therefore

$$\frac{C_{sh}}{A_p} = \frac{1}{\sqrt{2\pi}} \frac{\epsilon_0}{\lambda_D} \omega_p \tau_1 e^{-\eta} \{1 - \text{erf}[(-\eta)^{1/2}]\}. \quad (67)$$

One might think that the unknown constant  $\tau_1$  can be evaluated by matching smoothly to the solution for  $\eta > 0$ , but this is not the case. In the limit  $\eta \rightarrow 0$ ,

$$\frac{C_{sh}}{A_p} = \frac{1}{\sqrt{2\pi}} \frac{\epsilon_0}{\lambda_D} \omega_p \tau_1 \neq 0, \quad (68)$$

whereas  $C_{sh}$  at the space potential has to vanish because there is no sheath. Actually,  $C_{sh}$  has to drop to zero even from the electron saturation side. If  $T_i$  is finite, though very small, it begins to

be collected when  $-\eta$  is small, and Eq. (67) is no longer valid.  $C_{\text{sh}}$  will fall to zero as in Fig. 2, but much more steeply, in a voltage range scaled to  $T_i$  rather than  $T_e$ . Although the absolute magnitude of  $C_{\text{sh}}$  is not known, we can show its behavior according to Eq. (67) in Fig. 11. There is still a discontinuity at  $\eta = 0$ , but it is so spiky that it will not be seen, and  $C_{\text{sh}}$  will vary much more smoothly than in Fig. 5 when  $V_{\text{rf}}$  brings  $\eta$  into the electron saturation region.

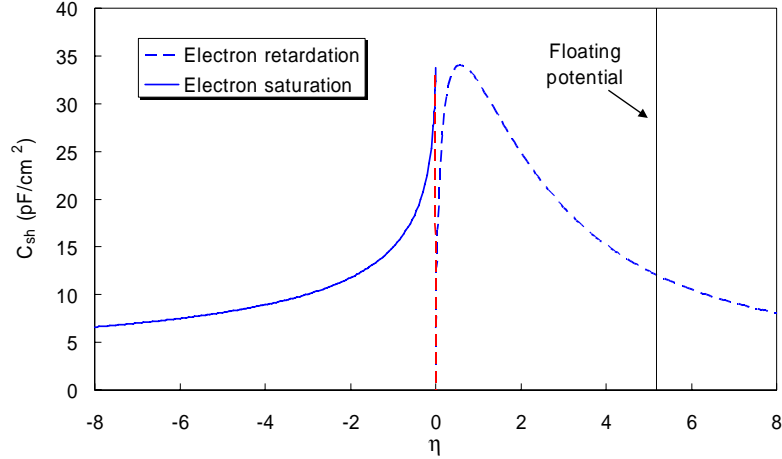


Fig. 11. Behavior of  $C_{\text{sh}}$  of a cylindrical electron sheath (—); the magnitude is approximate. Also shown for comparison is  $C_{\text{sh}}$  for a plane ion sheath (---) from Fig. 2. Both curves dip to 0 at the space potential.

The statement that the sheath vanishes at  $V_p = V_s$  does not hold when there is a dc magnetic field. The probe then casts a shadow, and particles are depleted from the tube of force intercepted by the probe. The space potential inside the tube is different from that outside, and it varies in a way that depends on the diffusion, classical or anomalous, of electrons across the B-field into the tube. Since  $V_p$  cannot be  $V_s$  everywhere, there is always going to be a sheath, and  $C_{\text{sh}}$  cannot vanish as it does for an infinitesimal probe in a B-field-free plasma.

A solution for  $C_{\text{sh}}$  in the Child-Langmuir approximation for cylinders ( $\eta \gg 1$ ) is also available<sup>18</sup>, but the series solution is quite cumbersome. For emission from a thin wire out to a sheath edge, Langmuir<sup>18</sup> showed that the solution is insensitive to  $s/r$  for  $s/r > 10$ . This may not be true for ion emission from the outer cylinder rather than the inner one. In any case this C-L solution cannot be connected to the electron retardation region without numerical integration.

## F. Conclusion

Both the real and imaginary parts of the sheath impedance of a Langmuir probe vary nonlinearly with rf fluctuations in space potential. An equation for the time-dependent sheath capacitance in plane geometry is derived including both the Child-Langmuir and Debye sheaths. Inclusion of the Debye sheath leads to violent oscillations of the sheath capacitance which may lead to generation of many harmonics of the rf frequency. For a cylindrical probe the sheath capacitance is given for the electron saturation region, but the transition region requires numerical integration. The effect of rf on probe characteristics can be minimized with an appropriate compensation circuit, whose parameters are specified.

This work was partially supported by the National Science Foundation Grant No. DMI-0115570.

## REFERENCES

- <sup>1</sup> M.A. Lieberman, IEEE Trans. Plasma Sci. **16**, 638 (1988).
- <sup>2</sup> M.A. Lieberman, IEEE Trans. Plasma Sci. **17**, 338 (1989).
- <sup>3</sup> V.A. Godyak and N. Sternberg, Proc. XX Int'l Conf. on Phenomena in Ionized Gases, Barga, Italy, July 8-12, 1991, p. 661 (1991).
- <sup>4</sup> V.A. Godyak and N. Sternberg, Phys. Rev. A **42**, 2299 (1990).
- <sup>5</sup> Y. Zhang, J. Liu, Y. Liu, and X. Wang, Phys. Plasmas **11**, 3840 (2004).
- <sup>6</sup> I.D. Sudit and F.F. Chen, Plasma Sources Sci. Technol. **3**, 162 (1994).
- <sup>7</sup> V.A. Godyak and R. B. Piejak, J. Appl. Phys. **68**, 3157 (1990).
- <sup>8</sup> R.R.J. Gagné and A. Cantin, J. Appl. Phys. **43**, 2639 (1972).
- <sup>9</sup> A. Cantin and R.R.J. Gagné, Appl. Phys. Lett. **30**, 316 (1977).
- <sup>10</sup> V.A. Godyak, R.B. Piejak, and B.M. Alexandrovich, Plasma Sources Sci. Technol. **1**, 36 (1992).
- <sup>11</sup> C.M.O. Mahony, P.D. Maguire, and W.G. Graham, Plasma Sources Sci. Technol. **14** 0 (2005).
- <sup>12</sup> F.F. Chen, Plasma Physics **7**, 47 (1965).
- <sup>13</sup> J.E. Allen, R.L. F. Boyd, and P. Reynolds, Proc. Phys. Soc. (London) **B70**, 297 (1957).
- <sup>14</sup> F.F. Chen and D. Arnush, Phys. Plasmas **8**, 5051 (2001).
- <sup>15</sup> J.G. Laframboise, University of Toronto Institute of Aerospace Studies Report No. 100 (June, 1966). National Technical Information Service Document No. AD634596.
- <sup>16</sup> H.M. Mott-Smith and I. Langmuir, Phys. Rev. **28**, 727 (1926).
- <sup>17</sup> F.F. Chen, *Electric Probes*, in "Plasma Diagnostic Techniques", ed. by R.H. Huddleston and S.L. Leonard (Academic Press, New York), Chap. 4, pp. 128-135 (1965).
- <sup>18</sup> I. Langmuir, Phys. Rev. **2**, 450 (1913).